Cholesterol-Metabolizing Enzyme Cytochrome P450 46A1 as a Pharmacologic Target for Alzheimer's Disease

Natalia Mast[a], Aicha Saadane[a], Ana Valencia-Olvera[a], James Constans[a], Erin Maxfield[a], Hiroyuki Arakawa[b], Young Li[a], Gary Landreth[c], and Irina A. Pikuleva[a1]

[a]Department of Ophthalmology and Visual Sciences, Case Western Reserve University, Cleveland, OH 44106, USA
[b]Behavioral Core, Case Western Reserve University, Cleveland, OH 44106, USA
[c]Stark Neuroscience Research Institute, Indiana University School of Medicine, Indianapolis, IN 46202, USA

[1]To whom correspondence should be addressed: Irina A. Pikuleva, Department of Ophthalmology and Visual Sciences, Case Western Reserve University, 2085 Adelbert Rd., Cleveland, OH 44106, Telephone: (216) 368-3823; FAX: (216) 368-0763; E-mail: iap8@case.edu

This is the author's manuscript of the article published in final edited form as:
Mast, N., Saadane, A., Valencia-Olvera, A., Constans, J., Maxfield, E., Arakawa, H., … Pikuleva, I. A. (2017). Cholesterol-metabolizing enzyme cytochrome P450 46A1 as a pharmacologic target for Alzheimer's disease. Neuropharmacology, 123, 465-476. https://doi.org/10.1016/j.neuropharm.2017.06.026

ABSTRACT

Cytochrome P450 46A1 (CYP46A1 or cholesterol 24-hydroxylase) controls cholesterol elimination from the brain and plays a role in higher order brain functions. Genetically enhanced *CYP46A1* expression in mouse models of Alzheimer's disease mitigates the manifestations of this disease. We enhanced CYP46A1 activity pharmacologically by treating 5XFAD mice, a model of rapid amyloidogenesis, with a low dose of the anti-HIV medication efavirenz. Efavirenz was administered from 1 to 9 months of age, and mice were evaluated at specific time points. At one month of age, cholesterol homeostasis was already disturbed in the brain of 5XFAD mice. Nevertheless, efavirenz activated CYP46A1 and mouse cerebral cholesterol turnover during the first four months of administration. This treatment time also reduced amyloid burden and microglia activation in the cortex and subiculum of 5XFAD mice as well as protein levels of amyloid precursor protein and the expression of several genes involved in inflammatory response. However, mouse short-term memory and long-term spatial memory were impaired, whereas learning in the context-dependent fear test was improved. Additional four months of drug administration (a total of eight months of treatment) improved long-term spatial memory in the treated as compared to the untreated mice, further decreased amyloid-β content in 5XFAD brain, and also decreased the mortality rate among male mice. We propose a mechanistic model unifying the observed efavirenz effects. We suggest that CYP46A1 activation by efavirenz could be a new anti-Alzheimer's disease treatment and a tool to study and identify normal and pathological brain processes affected by cholesterol maintenance.

Key words: CYP46A1, efavirenz, Alzheimer's disease, 24-hydroxycholesterol, amyloid, cholesterol

Highlights

- CYP46A1 activity was enhanced pharmacologically by the anti-HIV drug efavirenz.
- CYP46A1 activation promoted cholesterol turnover in the brain of 5XFAD mice.
- CYP46A1 activation reduced amyloid-β burden in the brain of 5XFAD mice.
- CYP46A1 activation reduced microglial immunoreactivity in the brain of 5XFAD mice.
- Efavirenz effects on behavior of 5XFAD mice were task- and treatment time-specific.

1. Introduction

CYP46A1 is the CNS-specific enzyme catalyzing cholesterol 24-hydroxylation, the major mechanism for cholesterol removal from the brain (Lund et al., 1999; Lutjohann et al., 1996). Normally, CYP46A1 resides in the endoplasmic reticulum and is expressed in neurons of the hippocampus, cortex, and cerebellum (Ramirez et al., 2008). In Alzheimer's disease, however, CYP46A1 shows prominent expression in astrocytes and around amyloid plaques (Bogdanovic et al., 2001; Brown et al., 2004). Plasma 24-hydroxycholesterol (24HC)[1], a marker of CYP46A1 activity in the brain (Lutjohann and von Bergmann, 2003), is increased at early disease stages (Lutjohann et al., 2000) and decreased with more advanced disease (Bretillon et al., 2000). Intronic polymorphisms are frequent in *CYP46A1* and present in ~29-40% of the population (http://www.ncbi.nlm.nih.gov/snp). Yet, only about half of linkage studies establish the *CYP46A1* association with Alzheimer's disease (Russell et al., 2009).

Genetic manipulations in mice provide evidence for a role of CYP46A1 beyond cholesterol homeostasis in the brain. Indeed, severe deficiencies in spatial, associative, and motor learning, and in hippocampal long-term potentiation were found in *Cyp46a1*$^{-/-}$ mice (Kotti et al., 2006). These deficiencies were related to the reduction in isoprenoid production during cholesterol biosynthesis, which was downregulated in response to CYP46A1 ablation (Kotti et al., 2008; Kotti et al., 2006). Conversely, the spatial memory retention was enhanced in aged female mice overexpressing *CYP46A1,* which also had an increased expression of receptors for N-Methyl-D-Aspartate (Maioli et al., 2013). The activation of these receptors is a key mediator of long-term potentiation (Sun et al., 2016b), and 24HC was discovered to serve as a positive allosteric modulator of N-Methyl-D-Aspartate receptors (Paul et al., 2013; Sun et al., 2016a). This discovery may explain, in part, improvements in cognitive function in several mouse models of Alzheimer's disease, in which CYP46A1 expression was increased either by a lack of a cholesterol esterifying enzyme ACAT1 (Bryleva et al., 2010) or by cerebral injections of the *CYP46A1*-containing adenovirus (Burlot et al., 2015; Hudry et al., 2010). In these models, CYP46A1 overexpression also ameliorated amyloid burden (Bryleva et al., 2010; Hudry et al., 2010) and was suggested to: 1) change cholesterol content in the endoplasmic reticulum and increase degradation of amyloid precursor protein (APP) in the endoplasmic membranes (Bryleva et al., 2010); 2) decrease cholesterol content in the lipid rafts of the plasma membranes and impair amyloidogenic APP processing (Hudry et al., 2010); and 3) inhibit by 24HC intracellular APP trafficking (Urano et al., 2013). Unlike overexpression, *Cyp46a1* downregulation (e.g., with a short hairpin *Cyp46a1* RNA) was found to be deleterious in normal mice, which exhibited cognitive deficits, elevated production of amyloid-β peptides and abnormal phosphorylation of tau (Djelti et al., 2015). Other studies reported neuronal sclerosis and epileptic activity in the hippocampus (Chali et al., 2015) and the phenotype of Huntington's disease with spontaneous striatal neuron degeneration and motor deficits (Boussicault et al., 2016).

Until recently, genetic manipulations were the only means whereby CYP46A1 activity was increased *in vivo*. We were successful with a different approach based on our studies of the biochemical and biophysical properties of CYP46A1 (Mast et al., 2004; Mast et al., 2010; Mast et al., 2009; Mast et al., 2012; Mast et al., 2003; Mast et al., 2013a, b; Shafaati et al., 2010; White et al., 2008). We discovered that CYP46A1 is an allosteric enzyme and that the administration of the anti-HIV medication efavirenz (EFV) to normal (C57BL/6J) mice activates CYP46A1 and cerebral cholesterol turnover in mouse brain (Anderson et al., 2016; Mast et al., 2014). Remarkably, the activating EFV dose in mice was only 0.09 mg/kg body weight (Mast et al., 2014), which is much lower than that (600 mg) given daily to HIV patients. Herein we administered EFV to 5XFAD mice, a model of rapid amyloidogenesis (Oakley et al.,

---

[1] The abbreviations used are: APP, amyloid precursor protein; EFV, efavirenz; 24HC, 24-hydroxycholesterol; Iba1, ionized calcium-binding adapter molecule 1; CS, conditioned stimulus; LXR, liver X receptors; MWM, Morris water maze; PBS, phosphate buffer saline; RNA-Seq, whole transcriptome sequencing; ThioS, Thioflavin S; US, unconditioned stimulus.

2006), and evaluated drug effects on cholesterol homeostasis in the brain, amyloid pathology, cognition and brain genome. We demonstrate that pharmacologic CYP46A1 activation reproduces the beneficial effects of *CYP46A1* overexpression accomplished by gene manipulations and thus could immediately be evaluated in a clinical trial. We also identified *Serpina1e* and *Serpina3k* encoding pro-inflammatory and pro-amyloidogenic proteins (Sardi et al., 2011) that have never been considered in the context of CYP46A1 activity, increased 24HC levels and the signaling *via* liver X receptors (LXR), transcription factors controlling the expression of cholesterol-related and other genes (Chawla et al., 2001). Increased cholesterol turnover and 24HC levels in the brain could be the key mediators of EFV effects.

2. Methods

2.1. Animals

5XFAD mice were obtained by crossing 5XFAD hemizygous males on B6SJL background with wild type B6SJL females (The Jackson Laboratory). Only F1 males or females homozygous for the transgenes were used. Age-and gender-matched animals on B6SJL background served as controls. The retinal degeneration allele *Pde6b^{rd1}* that leads to blindness was bred out of our colony. Mice were housed in the Animal Resource Center at Case Western Reserve University and maintained in a standard 12 h light/12 h dark cycle environment. Water and food were provided *ab libitum*. All animal procedures were approved by the Case Western Reserve University Institutional Animal Care and Use Committee and conformed to recommendations of the American Veterinary Association Panel on Euthanasia.

2.2. Chemicals

The S-isomer of efavirenz (EFV, brand name Sustiva) was purchased from Toronto Research Chemicals Inc.

2.3. EFV treatment

This was as described (Mast et al., 2014). Briefly, EFV was dissolved in drinking water at 0.42 mg/ml and provided to mice in light-protected bottles. On average, mice consumed every day 6.0-6.5 ml of EFV-containing water, which was similar to the consumption of regular water and represented a 0.1 mg/day/kg of body weight EFV dose for a 25-g mouse drinking daily 6.25 ml of water. EFV administration was initiated at 1 month of age, before the development of amyloid plaques (Oakley et al., 2006), and continued until animals were sacrificed for evaluations.

2.4. Brain processing

Mice were fasted overnight and next morning sacrificed. The brains were isolated as described (Mast et al., 2011) and either processed immediately or flash-frozen in liquid nitrogen and stored at -80^{o}C until further analyses. Left brain hemispheres were always used for sterol quantifications by isotope dilution gas chromatography-mass spectrometry following sample saponification (Mast et al., 2011). Right brain hemisphere were used for APP quantification by Western blot or amyloid-β peptide quantification by ELISA. The whole brains were used for histo- and immunohistochemistry stains after anesthetized mice were sequentially perfused through the heart with 30 ml of each, phosphate buffer saline (PBS) and 4% paraformaldehyde in PBS. The brains were then isolated, fixed for 4 days at room temperature in 4% paraformaldehyde in PBS, and transferred to 1% paraformaldehyde in PBS for storage at 4^{o} C.

2.5. Histo- and immunohistochemistry

The brain cryopreservation was as described (Corona et al., 2016), except the whole brain was used, and sagittal sections (10 µm-thick, cut at 1.2-1.5 mm from the midline) were mounted on slides prior to staining. Plaque abundance was analyzed as described (Corona et al., 2016), separately with 1% aqueous ThioS and primary mouse 6E10 antibody (1:1,000; Covance). For the latter, the antigen retrieval was in 88% aqueous formic acid solution for 3 min at room temperature. The 6E10 antibody was visualized with secondary goat anti-mouse Alexa Fluor 546 antibody (1:1,000; Life Technologies). The microglial cells were detected with primary rabbit antibody against ionized calcium-binding adapter molecule 1 (Iba1, 1:1,000; Wako) and secondary goat anti-rabbit Alexa Fluor 647 antibody (1:200, Jackson ImmunoResearch Inc.). All images were taken on an inverted microscope (DMI 6000 B, Leica Microsystems) that had a Retiga EXi-Fast camera (QImaging). The images were analyzed for the total number and combined area of the ThioS- and 6E10-positive plaques as well as Iba1-positive cells per whole brain cortex or hippocampus by the Metamorph Imaging Software (Molecular Devices). Only signals with the 2,000-16,383 intensity, a shape factor of ≥0.2, and size of plaques from 50 to 200 μm^2 for ThioS-stains and ≥80 μm^2 for 6E10-stains and were considered for the quantifications. Similarly, signals with the 1,500-16,383 intensity, a shape factor of ≥0.2, and a size of ≥100 μm^2 were considered for Iba1 quantifications.

2.6. Amyloid-β peptide quantifications

The right brain hemisphere was dissected from the cerebellum and brainstem followed by homogenate preparation as described (Schmidt et al., 2005). Soluble and insoluble amyloid-β peptides were extracted with 0.2% diethylamine and 70% formic acid, respectively, as described (Casali and Landreth, 2016), except 200 µl of the brain homogenate was used for extraction of insoluble amyloid-β peptides. The content of soluble and insoluble amyloid-β peptides was measured by a sandwich ELISA kit (KHB3482, Invitrogen) according to the manufacturer’s instructions.

2.7. Western blot analysis

Homogenates (10%, w/vol) from right brain hemispheres were prepared in 20 mM Tris-HCl, pH 7.4, containing 250 mM sucrose, 0.5 mM EDTA, 0.5 mM EGTA, and a cocktail of protease inhibitors (Complete, Roche). Tissue homogenization was followed by centrifugation at 1,500 g for 15 min and the SDS-PAGE separation of the supernatant obtained (4 or 8 µg protein/lane) on an 4-20% Tris/Glycine gradient gel (Bio-Rad) for APP quantification or 50 µg protein/lane on an 16% Tris/Tricine gel (Bio-Rad) for the C83 and C99 fragments quantification. A nitrocellulose membrane (Li-Cor) was used for protein transfer, and this membrane was blocked with Li-Cor blocking buffer (Li-Cor) containing 0.1% Tween-20. APP was visualized with primary mouse monoclonal antibody against the APP N-terminus (Anti-APP A4 clone 22C11, 1:10,000; EMD Millipore) (Saito et al., 2014) and secondary goat anti-mouse antibody IRDye 800CW (1:20,000; Li-Cor). Beta actin was used as a loading control and was detected with primary rabbit polyclonal antibody (1:500; Abcam) and secondary goat anti-rabbit antibody IRDye 680RD (1:20,000, Li-Cor). C83 and C99 were visualized with primary rabbit polyclonal antibody against the APP C-terminus (A8717, 1:4,000; Sigma-Aldrich) (Saito et al., 2014) and secondary goat anti-rabbit antibody IRDye 680RD (1:20,000, Li-Cor). GAPDH was used as a loading control and was detected with primary mouse polyclonal antibody (1:5,000; Abcam) and secondary goat anti-mouse antibody IRDye 800CW (1:20,000; Li-Cor). Membranes were imaged by the Odyssey infrared imaging system (Li-Cor).

2.8. Behavioral tests

Untreated and treated 5XFAD mice for evaluations at 5 month of age (each cohort of 4 females and 12 males) were tested individually for the following tasks: Y-maze at day1; Morris water maze (MWM) at days 2-6; and fear conditioning memory tests at days 12 and 13 after the break at days 7-11. The Y-maze test was performed for a short-term, working memory task as described (Arakawa et al., 2014;

Bryan et al., 2010) utilizing a Y-shaped maze with an arm length of 35 cm, width of 6 cm, and height of 10 cm. Each mouse was tested for 5-14 min until the animal made 20 arms choices. The choices of entered arms were then calculated to determine the alternation rate, i.e., degree of arm entries without repetitions. The MWM test evaluated a long-term spatial memory (Yu et al., 2014). Mice had to find an invisible platform when swimming in a pool. Three trials per day were performed for five consecutive days. Swim time and path length were recorded using an automated tracking software (ANY-maze, Stoelting Co.). Latencies to reach the platform during each trial were wrapped up into one day-block of three trials, which represented a long-term spatial learning. In addition, the fear-related memory tests including both context- and cue-dependent versions were performed (Ulatowski et al., 2014). Briefly, mice were placed in a conditioning box (Med Associates) and trained to associate the conditioned stimulus (CS, a pure tone of 3kHz, 80 dB for 30 sec) with co-terminated unconditioned stimulus (US, electrical shock of 0.5 mA for 1 sec). This fear conditioning procedure was repeated four times with 120-sec accumulation and 60-sec inter-stimulus-interval. Twenty-four hours later, mice were placed back in the box with a same context and their freezing behavior in the absence of CS was measured for 5 min (context-dependent fear). Two hours after the context fear test, mice were reintroduced into the contextually altered box (shape, lighting, and odor) so that they could no longer recognize the chamber, in which they had been trained. Freezing behavior was measured during the first 3 min without the tone (non-CS) and then during the second 3 min with the tone (CS).

Untreated and treated 5XFAD mice for evaluations at 9 month of age comprised of 13 females and 1 male in the untreated group and 13 females and 5 males in EFV-treated group. The behavioral tests were the same as at 5 months of age.

2.9. Whole brain transcriptome sequencing (RNA-Seq)

One hemisphere from each of three 5XFAD mice per group (EFV-treated and untreated) was homogenized in 10 vol (w/v) of TRIzol reagent (Life Technologies) followed by the isolation of total RNA according to the manufacturer's protocol. Individual libraries were then prepared from each RNA sample (500 ng in 10 µl) using the TruSeq Stranded Total RNA with RiboZero Gold kit (Illumina). Each library was individually tagged with a unique adapter-index and pooled together. Pooled libraries were run on a HiSeq 2500 System (Illumina) with 2 x 100 bp paired-end reads, and the quality of sequencing reads was assessed by the FastQC softwrae (Babraham Bioinformatics). Reads that passed the quality filters were aligned to the mouse mm10 reference genome using the TopHat software (Trapnell et al., 2009), which implements the Bowtie 2 algorithm (Langmead and Salzberg, 2012) for sequence alignment and analyzes the mapped reads to identify splice junctions between exons. The TopHat results were analyzed using the Cufflinks RNASeq analysis package (Trapnell et al., 2010), and the fragments per kilobase of exon per million fragments mapped values were reported for each gene and sample. Differentially expressed genes between the control and treatment group were identified using a q-value (adjusted p-value for multiple testing) of ≤0.05.

2.10. qRT-PCR

Total RNA (1 µg) was converted to cDNA by SuperScript III Reverse Transcriptase (Invitrogen) and used for qRT-PCR conducted on an ABI PRISM 7000 Sequence Detection System (Applied Biosystems). The sequences of the primers for gene quantifications was taken from qPrimerDepot, a primer database for qRT-PCR (Cui et al., 2007). PCR reactions were performed in triplicate and normalized to β-actin.

2.11. Statistical analysis

All graphs represent mean ± SD, except behavioral tests, where the error bars are SEM. Data analysis is indicated in each figure legend and represents either unpaired Student's t-test assuming a two-tailed distribution or a two-way ANOVA. Statistical significance was considered when P values were ≤ 0.05.

All histo- and immunohistochemistry images and Western blots are representative of observations in 3-8 mice/per group.

3. Results

3.1. Cholesterol homeostasis in the 5XFAD brain is disturbed by the transgene expression but is responsive to EFV treatment

Three groups of animals (the background B6SJL strain, untreated and EFV-treated 5XFAD mice) were assessed after weaning (from 1 month of age) for monthly brain levels of cholesterol, two cholesterol precursors (lathosterol and desmosterol) and one cholesterol metabolite (24HC). Lathosterol and desmosterol are the markers of cholesterol biosynthesis in neurons and astrocytes, respectively (Pfrieger and Ungerer, 2011), whereas 24HC reflects cholesterol elimination from the brain, realized mainly *via* 24-hydroxylation mediated by CYP46A1 (Lund et al., 1999; Lutjohann et al., 1996). In B6SJL mice, a pool of cerebral cholesterol expanded until 3 months of age (Fig. 1A), whereas the cholesterol biosynthesis rates (the lathosterol and desmosterol levels) declined after birth (Fig. 1B,C) and the 24HC levels were not changing with age (Fig. 1D). Yet, after 3 months of age, i.e., in the adult brain, the levels of all measured sterols became steady state, consistent with previous findings in other strains of normal mice (Dietschy and Turley, 2004; Lund et al., 1999; Quan et al., 2003). The data obtained reveal the mechanism whereby cholesterol biosynthesis is balanced by cholesterol metabolism in the adult mouse brain; it is through a reduction in the rate of prenatal cholesterol biosynthesis (Fig. 1B,C) rather than an increase in the rate of postnatal 24HC production (Fig. 1D).

Cholesterol content and sterol dynamics were different in the brain of untreated 5XFAD mice (Fig. 1E-H). After weaning, cerebral cholesterol was lower in these animals than in B6SJL mice, and reached the levels of the B6SJL brain only by 8 months of age (Fig. 1E,M). Brain lathosterol, initially the same in the weaned 5XFAD and B6SJL animals, decreased with age in both strains (Fig. 1F,N). Yet in 5XFAD mice this decrease was not as steep as in the B6SJL strain reaching the B6SJL levels only at 6-8 months. Then, at 9 months of age, the 5XFAD brain lathosterol began to increase again. The desmosterol levels were always higher in the 5XFAD brain than in the B6SJL brain and never reached those in the B6SJL strain (Fig. 1G,O). Finally, the 24HC levels were increased at 2-4 months in the untreated 5XFAD brain and then became similar to those in the B6SJL brain (Fig. 1H,P). Thus, not only was brain cholesterol lower in adult 5XFAD mice, but all measured sterols fluctuated with age, and the changes in cholesterol precursors and 24HC were not parallel. Such sterol pattern suggests that the overexpression of mutant human APP and/or presenilin 1 disturbed cholesterol homeostasis in the 5XFAD brain, and periodically uncoupled cholesterol biosynthesis from cholesterol elimination.

Despite the dysregulation, cholesterol homeostasis in the brain of 5XFAD mice responded to the EFV treatment. As compared to untreated 5XFAD mice, the drug led to a statistically significant increase in the brain 24HC levels beginning from 5 months of age, reflective of the activation of CYP46A1 (Fig. 1L,P) and consistent with our previous studies in C57BL/6J mice (Mast et al., 2014). However, in young, 2-4 month old animals this increase was apparently not compensated by the cholesterol biosynthetic processes, and cholesterol was depleted from the brain of EFV-treated mice (Fig. 1I,M). Then, at 4-6 months of age, cerebral cholesterol biosynthesis in EFV-treated mice probably became coupled to cerebral cholesterol metabolism, and cholesterol content in the brain began to increase. At 6 months, cerebral cholesterol in EFV-treated 5XFAD mice finally reached the sterol levels in the brain of the B6SJL mice and was subsequently stable. In contrast, in the untreated 5XFAD brain, cholesterol levels reached those of the B6SJL strain 2 months later. Thus, pharmacologic activation of CYP46A1 is possible in the brain with disturbed cholesterol maintenance and leads to a faster normalization of brain cholesterol.

On the basis of the data obtained, we selected two time points (5 and 9 months of age) for more expanded assessments in 5XFAD mice. At both time points, cerebral cholesterol was similar in EFV-untreated and treated 5XFAD mice. Yet at 5 months of age, both groups had their cerebral cholesterol lower than in B6SJL mice and cholesterol levels were still unstable. In contrast, at 9 months age, cerebral cholesterol was similar in all three groups of mice and already stabilized in 5XFAD animals. Another important difference between the two evaluation time points was that the 5 month-evaluations were preceded by a cholesterol depletion from the brain EFV-treated mice, whereas the 9 month-evaluations were preceded by increases in cerebral 24HC and cholesterol turnover (Fig. 1M-P).

3.2. EFV treatment reduced amyloid-β pathology and microglial immunoreactivity in 5XFAD mice

The brain amyloid burden was assessed by Thioflavin S (ThioS) staining, immunohistochemistry using the antibody 6E10, and ELISA quantifications (Figs. 2,3). ThioS binds to β sheet-rich structures and visualizes amyloid dense-core plaques observed at later stages of Alzheimer's disease (Dickson, 1997). 6E10 interacts with amyloid-β peptides, APP and its fragment soluble APPα and detects amyloid diffuse-core plaques prevalent in the preclinical stages of the disease (Rozemuller et al., 1989). Four months of EFV treatment reduced amyloid abundance in the brain cortex and hippocampus of 5-month old 5XFAD mice (Figs. 2,3), the two regions that are among those affected most severely in Alzheimer's disease and the first to show amyloid deposition in 5XFAD mice (Oakley et al., 2006). In the cortex, the total number and area of the ThioS-positive plaques was reduced by 35% and 45%, respectively (Fig. 2B). In the hippocampus, these reductions were by 33% and 38%, respectively. The 6E10-positive plaques showed statistically significant reductions in the total number and area in the cortex (by 50% and 70%, respectively), and in total area in the hippocampus (by 72%, Fig. 3B). The total number of the 6E10-positive plaques was not significantly reduced in the hippocampus. Thus, both diffuse- and dense-core amyloid plaques were reduced by EFV treatment in the cortex, whereas changes in the hippocampus were plaque morphology-dependent.

Immunolabeling for 6E10 was conducted simultaneously with that for Iba1, upregulated in activated microglial cells that surround amyloid plaques (Dickson, 1997). EFV-treatment reduced the number of Iba1-positive cells by 45% in the cortex and 64% in the hippocampus; similarly, a total immunoreactivity for Iba1 was reduced by 49% and 78% in the cortex and hippocampus, respectively (Fig. 3B).

The measurements by ELISA were used to discriminate between the amyloid-$\beta_{1\text{-}40}$ and amyloid-$\beta_{1\text{-}42}$ species as well as between soluble and insoluble amyloid-β peptides. Insoluble amyloid-$\beta_{1\text{-}42}$ peptide is predominant in the 5XFAD mice and the initial amyloid species that deposit into amyloid plaques in all forms of Alzheimer's disease (Haass and Selkoe, 2007). Four and eight months of EFV treatment led to the same, ~30%, statistically significant reduction in the levels of insoluble amyloid-$\beta_{1\text{-}42}$ peptide. In addition, a 40% reduction in the levels of insoluble amyloid-$\beta_{1\text{-}40}$ peptide was observed after eight months of treatment (Fig. 3C,D). Neither treatment time affected significantly the soluble amyloid-β species. ELISA quantifications supported histo- and immunohistochemistry data.

3.3. EFV treatment reduced the mortality rates in 5XFAD male mice

The mortality rates were determined based on animal survival in the cohorts of animals assigned for behavioral tests. The cohort of 5XFAD mice for evaluations at 5 month of age (after 4 months of EFV administration to the treated group) comprised initially of 4 females and 16 males in the untreated group and 4 females and 14 males in EFV-treated group. By 5 months of age, there was no mortality among any of the female mice and in contrast 25% (four animals) and 14% (2 animals) of mortality among male mice in the untreated and EFV-treated groups, respectively.

The cohort of 5XFAD mice for evaluations at 9 month of age comprised initially from 13 females and 8 males in the untreated group and 15 females and 5 males in EFV-treated group. By 9 months of age (after 8 months of EFV administration to the treated group), there was no mortality among female mice in the untreated group and 13% of mortality (two animals) in EFV-treated group. The male mortality was 87% in the untreated group (7 animals) and zero in EFV-treated group.

3.4. EFV effects on behavior of 5XFAD mice were task- and treatment time-specific

EFV effects were assessed on only those memory tasks that are known to be impaired in the 5XFAD strain: Y-maze, MWM, and conditioned fear tests (Oakley et al., 2006; Ohno et al., 2006). In the Y-maze test, which refers to hippocampus-dependent short-term spatial memory, EFV treatment had little impact on memory performance. The alteration rate was slightly reduced after 4 months of drug treatment and was similar in the untreated and treated groups after 8 months of EFV administration (Fig. 4A). In the MWM test, a long-term spatial memory test, no learning through the trials was observed in the treated group after 4 months of EFV administration whereas the untreated group of the same age (5-month old) displayed steadily increasing learning performance (Fig. 4B). However, the treated group showed better learning performance than the untreated controls when tested after 8 months of EFV treatment at 9 months old. Moreover, the treated 9-month old mice even demonstrated some resistance to age-related behavioral deterioration that is known to occur in 5XFAD mice (Schneider et al., 2014). Thus, in both short-term and long-term spatial memory tasks, the direction of the effect of treatment on memory performance reversed with age and improved in MWM in mice older than 5 months. Fear conditioning test, which refers to emotional memory tasks, provided further insight into short-term and long-term EFV effects on 5XFAD mice. Cue-dependent conditioning is based on associative learning among stimuli, which are mainly regulated by the amygdala-thalamo-cortical pathway; context-dependent conditioning is regulated by amygdalar–hippocampal communication (Orsini and Maren, 2012). Five- and nine-month old EFV-treated and untreated 5XFAD mice showed a similar freezing response to the US exposures during training (Fig. 4C). Nevertheless, the 5-month old EFV-treated mice had a greater percentage of freezing in the context-dependent fear test than the untreated mice of the same age, and the 9-month old EFV-treated mice displayed a similar level of freezing as untreated controls (Fig. 4D). In the cue-dependent fear test, there was no difference between the treated and untreated groups at either 5- or 9-months of age (4 and 8 months of EFF treatment, respectively, Fig. 4E). The results of the context-dependent memory performance in 5-month old EFV-treated mice indicate an enhanced fear of context (inaccurate target) rather than cue (accurate target) after 4- but not 8-months of EFV treatment.

3.5. EFV treatment reduces brain APP levels and gene expression in 5XFAD mice

An increase by genetic means of cerebral 24HC levels decreased the APP levels (Bryleva et al., 2010) and/or altered APP processing (Bryleva et al., 2010; Hudry et al., 2010) in mouse models of Alzheimer's disease. Similarly, when treated with EFV, the APP levels were decreased in the 5XFAD model as well, by 40% (P = 0.03) and 30% (P = 0.15) at 5 and 9 months of age, respectively (Fig. 5A,D). Yet, the APP processing did not seem to be affected by EFV treatment as indicated by the quantifications of the APP cleavage fragments C99 and C83, produced as a result of amyloidogenic and non-amyloidogenic processing, respectively. C99 and C83, clearly visible in only 9-month old 5XFAD mice (Fig. 5E), showed a trend to a decrease upon EFV treatment when quantified individually (by 33% for C99, P = 0.06, and by 35% for C83, P = 0.07), and a statistically significant decrease by 35% (P = 0.02), when quantified as the sum (Fig. 5F). The extent of these decreases (33-35%, Fig. 5F) was similar to that of APP (by 30%, Fig. 5D) suggesting that the C83 and C99 decreases is a consequence of the APP reduction and that neither amyloidogenic nor non-amyloidigenic APP processing was affected by EFV treatment, an interpretation also supported by the unchanged C83 to C99 ratio.

24HC is a potent activator of the transcription factors LXR receptors (Chen et al., 2007; Janowski et al., 1996), which control gene expression *via* activation, repression and transrepression (Saijo et al., 2013). Hence, we assessed cerebral gene expression by whole transcriptome sequencing (RNA-Seq). About 22,560 genes were detected at 5 months in the 5XFAD brain, which represent ~90% of the mouse transcriptome (Fig. 5B). Of these genes, 13 had at least a 2.5-fold difference (an arbitrary cut off) in expression between EFV-treated and untreated 5XFAD mice and the positive false discovery rate $q \leq 0.05$. All 13 genes were downregulated (3.2-4.7-fold) in EFV-treated mice, and 9 of them were of relevance to Alzheimer's disease: *Alb* (albumin) (Stanyon and Viles, 2012), *Pomc* (Pro-opiomelanocortin)

(Leone et al., 2013), *Serpinas 3k* and *1e* (Serpin Peptidase Inhibitor 3 and 1, respectively) (Guan et al., 2012; Maes et al., 2006), *GC* (Group-Specific Component or Vitamin D Binding Protein) (Moon et al., 2013), *Apoa1 and Apoa2* (Apolipoproteins A-I and A-II) (Lewis et al., 2010; Song et al., 2012), *Apob* (Apolipoprotein B) (Loffler et al., 2013; Namba and Ikeda, 1991), and *Cyp2e1* (Cytochrome P450 2E1) (Van Ess et al., 2002). The 9 genes of relevance to Alzheimer's disease were then assessed by qRT-PCR, which confirmed their decreased expression, from 5- to 15-fold in EFV-treated mice (Fig. 5C). Thus, EFV treatment affected gene expression, but none of the affected genes was the known target regulated by LXR activation; either these genes are indirect LXR targets or downregulated as a result of a reduced amyloid load due to EFV treatment.

4. Discussion

The present study led to several major findings. First, cholesterol homeostasis is disturbed in the brain of 5XFAD mice, a widely used Alzheimer's disease model. Second, a very low dose of the anti-HIV drug EFV stably activates CYP46A1 and promotes cholesterol turnover in the 5XFAD brain. Third, CYP46A1 activation leads to a faster cholesterol homeostasis normalization in the 5XFAD brain. Finally, EFV treatment reduces amyloid-β burden as well as microglia activation in the brain of 5XFAD mice and ultimately improves mouse performance in MWM.

Previous work on a different mouse model of Alzheimer's disease linked transgenic expression of mutant human APP and presenilin 1 and the alterations in brain cholesterol homeostasis (Vanmierlo et al., 2010). Our sterol measurements (Fig. 1) are consistent with this link and suggest that several mechanisms can underlie dysregulation of cholesterol homeostasis in the 5XFAD brain. Prenatally, this is probably the APP overexpression, while postnatally, there is also a contribution of amyloid deposition. Indeed, cholesterol lowering in the 5XFAD brain (Fig. 1M) preceded the appearance of amyloid deposits at postnatal month 2 (Oakley et al., 2006), suggesting that it is likely the transgene expression that decreases initially cholesterol levels in the 5XFAD brain. This explanation is supported by studies in cultured neurons but not astrocytes showing that APP can interact with the transcription factor SREBP1 and prevent SREBP1 from maturation (Pierrot et al., 2013), thus decreasing cerebral cholesterol by decreasing cerebral cholesterol biosynthesis controlled by SREBPs. Also, *in vitro*, cholesterol was shown to bind to APP and affect its cleavage by the secretases (Barrett et al., 2012). Accordingly, cholesterol lowering in the 5XFAD brain can be due in part to cholesterol interaction with APP, the mechanism which will complement the APP-mediated reduction of the cholesterol biosynthesis rates. However, the APP lowering effect on cholesterol biosynthesis in the 5XFAD brain should be counteracted at some time point by another mechanism (likely SREBP maturation) to prevent cholesterol depletion. If operative in growing 5XFAD mice, this mechanism should lead to a slower decline in the cholesterol biosynthesis rates as compared to the B6SJL mice, exactly the effect that was observed in 2- and 3-month old animals (Fig. 1N). Prenatally, cholesterol input is not coupled to cholesterol elimination because CYP46A1 is barely detectable in the brain at postnatal week 1 and reaches its maximal expression only 2-3 weeks later (Lund et al., 1999). Accordingly, it is plausible that cholesterol homeostasis in the 5XFAD brain is dysregulated at birth because prenatal mechanisms controlling cholesterol biosynthesis rates are not well coordinated with and are not well compensated by cholesterol elimination.

Besides high levels of APP, the 5XFAD brain has a progressive amyloid deposition over the period of 2 to 9 month of age (Oakley et al., 2006). In cell culture, amyloid-$\beta_{1\text{-}40}$ peptide was found to inhibit cholesterol biosynthesis by inhibiting HMGCR, the rate-limiting enzyme in the production of cholesterol (Grimm et al., 2005). Also in cell culture, amyloid-$\beta_{1\text{-}42}$ was demonstrated to reduce the levels of mature SREBP-2 and affect cholesterol biosynthesis (Mohamed et al., 2012). It is conceivable that these and probably other processes (Grosgen et al., 2010) can further disturb cholesterol maintenance in the 5XFAD brain, which is already compromised prenatally by the transgene expression. As a result, cholesterol input and output in the adult 5XFAD brain are periodically uncoupled leading to the fluctuations of cerebral cholesterol (Fig. 1E). Only by 8 months of age, when amyloid deposition starts to level off, cholesterol levels in the 5XFAD brain reach those in the B6SJL brain and the cholesterol-related processes seem to become coordinately regulated.

Despite aberrant cholesterol homeostasis, EFV dose ~100-times lower than that given to HIV patients (~0.1 mg/day/kg *vs* ~10 mg/day/kg) stably activated CYP46A1 in the 5XFAD brain (Fig. 1L,P). Importantly, this activation ultimately led to a compensatory increase in cerebral lathosterol but not desmosterol suggesting that it is cholesterol biosynthesis and turnover in neurons rather than astrocytes that mostly became enhanced. This result is consistent with normally neuron-specific CYP46A1 expression in mice (Ramirez et al., 2008) and points to CYP46A1 as the primary EFV target. If so, cholesterol depletion from the brain of 2-4-month old EFV-treated mice was likely from neurons, thus providing an explanation for mixed results of behavioral tests on 5-month old 5XFAD mice after 4 months of EFV treatment (Fig. 4). This treatment worsened mouse learning in Y-maze and MWM, improved mouse performance in the context-dependent fear test, and had no effect on the cue-dependent fear test. Conversely, no worsening in all three memory tests was detected in 9-month old 5XFAD mice after 8 months of EFV treatment, and the treatment significantly improved mouse learning in MWM. The eight-month treatment time even seemed to slow down behavioral deterioration related to age (Fig. 5B). EFV effects after 4 months of treatment may be confounded by the brain cholesterol depletion during the two months preceding behavioral evaluations (Fig. 1M). This depletion could be a result of the treatment starting when cholesterol pool in mouse brain was still expanding and cholesterol biosynthesis and metabolism were poorly coupled. In addition, there may be also the effect of the transgene expression. The former interpretation is supported by a lack of cholesterol depletion in the brain of normal C57BL/6J mice, whose treatment started at the age of 3 months, when cerebral cholesterol homeostasis was already stable (Mast et al., 2014). Yet, at 9 months of age, cerebral cholesterol was similar in EFV-treated and untreated 5XFAD mice for already 2 months prior to testing, and the confounding cholesterol reduction was absent. Alternatively, behavioral impairment could be a result of a neurotoxic effect of 24HC, whose small spike was observed in 5-month old 5XFAD mice after 4 months of EFV treatment (Fig. 1O). Some but not all studies in cell culture reported that 24HC may be cytotoxic (Kolsch et al., 1999) as well as potentiate the pro-apoptotic and pro-necrotic effects of amyloid-β_{1-42} peptide (Ferrera et al., 2008; Gamba et al., 2011). Regardless of the effect, enhanced cholesterol turnover in the brain with or without subsequent cholesterol depletion could be a tool to study and identify normal and pathological brain processes affected by cholesterol maintenance.

Three cerebral sterols (cholesterol, lathosterol, and 24HC) as well as cholesterol turnover were modulated in EFV-treated 5XFAD mice raising a question of how these sterols, each or collectively, contributed to the observed amelioration of amyloid pathology. Cerebral cholesterol was shown to regulate the production and amount of the amyloid-β peptides *in vitro* and cell cultures by modulating the activities of α- β-, and γ-secretases (Grosgen et al., 2010; Vance, 2012). Nevertheless, we do not believe that changes in cerebral cholesterol content were the underlying reason for a reduction in amyloid burden. First, the reductions of cellular/membrane cholesterol that modulated the secretase activities were massive (up to 70%) (Fassbender et al., 2001; Kojro et al., 2001; Simons et al., 1998; Wahrle et al., 2002). By contrast, in our 2-4 month old EFV-treated mice, the reductions of total cerebral cholesterol were much smaller, from 17% to maximum 37% (Fig. 1M). Second, the extent of the amyloid-β_{1-42} reduction was similar at 5 and 9 months age, despite at 5 months, cerebral cholesterol was much lower than at 9 months (Fig. 1M) as were the peptide accumulations (Fig. 4C,D).

Only 24HC and cholesterol turnover were increased to the same extent in 5- and 9-month old EFV-treated 5XFAD mice (Fig. 1N,P) leading to a possible mechanistic model, which unifies EFV effects (Fig. 6). In this model, EFV treatment activates CYP46A1 (Event 1) and increases the brain 24HC levels (Event 2) as well as the brain cholesterol turnover rate (Event 3). The latter increases cholesterol flux through the cellular membranes and inhibits APP processing (Event 4) *via* disruption of lipid rafts required for APP processing (Simons et al., 1998). Unprocessed APP is rapidly degraded (Chia and Gleeson, 2011), thus decreasing the APP levels (Fig. 5A,D). Increased 24HC content could also decrease the APP levels (Event 3') *via* inhibition of APP processing by non-membrane related mechanisms (Brown et al., 2004). Increases in both 24HC and cholesterol turnover rate could have beneficial effects on mouse performance in MWM (Events 3'' and 4') because of the suggested role of 24HC as a positive allosteric modulator of N-Methyl-D-Aspartate receptors (Paul et al., 2013; Sun et al., 2016a) and the role of the brain cholesterol turnover rate in the long term potentiation (Kotti et al., 2008; Kotti et al., 2006). Finally, 24HC can bind to LXRs (Event 3''') (Chen et al., 2007; Janowski et al., 1996) and blunt the induction of pro-inflammatory genes in brain astrocytes, peripheral macrophages, and microglial cells (Joseph et al., 2003; Kim et al., 2006; Lee et al., 2009; Zhang-Gandhi and Drew, 2007) *via* transrepression (Events 5, 5', and 5''). In astrocytes (Event 5), the downregulated genes include IL-1β (Zhang-Gandhi and Drew, 2007), which along with TNFα controls the expression of *SERPINA3* (Das and Potter, 1995; Gitter et al., 2000; Machein et al., 1995; Morihara et al., 2005), human ortholog of *Serpina3k* (Heit et al., 2013) encoding α-1-antichymotrypsin. Reduced expression of α-1-antichymotrypsin may reduce amyloid pathology (Events 7 and 8) because α-1-antichymotrypsin was shown to directly bind to amyloid-β peptides and enhance their fibrillization and thereby plaque formation (Abraham and Potter, 1989; Eriksson et al., 1995; Ma et al., 1996; Ma et al., 1994). The LXR-mediated transrepression of inflammatory genes can also explain a decrease in microglia activation (Event 5'') and downregulation of *Serpina1e* encoding α-1-antitrypsin (Event 5'). The expression of the target genes that are upregulated by LXRs, however, was not changed in mRNA-Seq (Fig. 5B), possibly due to a local, namely cell- and region-specific gene upregulation in astrocytes and microglia around amyloid plaques. Accordingly, these small changes in gene expression were not detected by RNA-Seq, which was conducted on whole brain homogenates. Alternatively, gene activation by LXRs was not operative upon EFV treatment, consistent with a lack of gene upregulation in *CYP46A1* transgenic mice (Shafaati et al., 2011).

Several general similarities in the effects on the brain could be found between 5XFAD mice treated with EFV and animals with increased *CYP46A1* expression due to: 1) genetic ablation of *Acat1* in mice transgenic for mutant human *APP*, *PS1*, and *MAPT* (Bryleva et al., 2010); or 2) cerebral injections of the *CYP46A1*-containing adenovirus to APP23 mice (Hudry et al., 2010). In all three cases, the content of 24HC in the whole brain or injected brain regions was increased, at least at the tested time points, whereas the amyloid-β_{1-42} levels were decreased, and cognitive deficits were ameliorated. Additional similarities include the APP reduction in EFV-treated 5XFAD mice and *Acat1*$^{-/-}$ triple transgenic mice, and the reduction in microglia activation in EFV-treated 5XFAD mice and *CYP46A1*-vector injected APP23 mice. The differences also appear to exist but are difficult to directly compare due to different experimental set ups, evaluation times, and transgenic mouse modes used.

In summary, oral administration of a small dose of the anti-HIV drug EFV to a mouse model of Alzheimer's disease ameliorated amyloid pathology in the brain and led to changes supporting therapeutic potential of cholesterol-metabolizing enzyme CYP46A1, its metabolite 24HC and 24HC-mediated LXR transrepression of some of the inflammatory genes in astrocytes and microglia surrounding amyloid plaques.

5. Conclusions

Collectively, our findings support the potential of CYP46A1 as a pharmacologic target for Alzheimer's disease and that EFV should be tested for CYP46A1 activation in a clinical trial.

Author contributions

NM, AS, AVO, JC, EM, HA, and YL conducted experiments; NM, JC, EM, HA, GL, and IP analyzed the data; IP wrote the manuscript.

Funding

This work was supported in part by United States Public Health Service Grant GM62882 (to I.A.P) and the Core Grant P30 EY11373. I.A.P. is a Carl F. Asseff Professor of Ophthalmology

Conflict of interests

The authors have declared that no conflict of interest exists.

Acknowledgements

We thank B. Casali and Monica Holle for help with mastering brain immunohistochemistry techniques and ELISA assays; Case Genomics Core for RNA-Seq, and the Visual Sciences Research Center Core Facilities for assistance with mouse breeding (Heather Butler and Kathryn Franke), animal genotyping (John Denker), tissue sectioning (Catherine Doller), and microscopy (Dr. Scott Howell and Anthony Gardella).

References

Abraham, C. R., Potter, H., 1989. The protease inhibitor, alpha 1-antichymotrypsin, is a component of the brain amyloid deposits in normal aging and Alzheimer's disease. Ann. Med. 21, 77-81.

Abraham, C. R., Selkoe, D. J., Potter, H., 1988. Immunochemical identification of the serine protease inhibitor alpha 1-antichymotrypsin in the brain amyloid deposits of Alzheimer's disease. Cell 52, 487-501.

Akiyama, H., Barger, S., Barnum, S., Bradt, B., Bauer, J., et al., 2000. Inflammation and Alzheimer's disease. Neurobiol. Aging 21, 383-421.

Anderson, K. W., Mast, N., Hudgens, J. W., Lin, J. B., Turko, I. V., et al., 2016. Mapping of the allosteric site in cholesterol hydroxylase CYP46A1 for efavirenz, a drug that stimulates enzyme activity. J. Biol. Chem. 291, 11876-11886.

Arakawa, H., Suzuki, A., Zhao, S., Tsytsarev, V., Lo, F. S., et al., 2014. Thalamic NMDA receptor function is necessary for patterning of the thalamocortical somatosensory map and for sensorimotor behaviors. J. Neurosci. Methods 34, 12001-12014.

Barrett, P. J., Song, Y., Van Horn, W. D., Hustedt, E. J., Schafer, J. M., et al., 2012. The amyloid precursor protein has a flexible transmembrane domain and binds cholesterol. Science 336, 1168-1171.

Bogdanovic, N., Bretillon, L., Lund, E. G., Diczfalusy, U., Lannfelt, L., et al., 2001. On the turnover of brain cholesterol in patients with Alzheimer's disease. Abnormal induction of the cholesterol-catabolic enzyme CYP46 in glial cells. Neurosci. Lett. 314, 45-48.

Boussicault, L., Alves, S., Lamaziere, A., Planques, A., Heck, N., et al., 2016. CYP46A1, the rate-limiting enzyme for cholesterol degradation, is neuroprotective in Huntington's disease. Brain 139, 953-970.

Bretillon, L., Siden, A., Wahlund, L. O., Lutjohann, D., Minthon, L., et al., 2000. Plasma levels of 24S-hydroxycholesterol in patients with neurological diseases. Neurosci. Lett. 293, 87-90.

Brown, J., 3rd, Theisler, C., Silberman, S., Magnuson, D., Gottardi-Littell, N., et al., 2004. Differential expression of cholesterol hydroxylases in Alzheimer's disease. J. Biol. Chem. 279, 34674-34681.

Bryan, K. J., Mudd, J. C., Richardson, S. L., Chang, J., Lee, H. G., et al., 2010. Down-regulation of serum gonadotropins is as effective as estrogen replacement at improving menopause-associated cognitive deficits. J. Neurochem. 112, 870-881.

Bryleva, E. Y., Rogers, M. A., Chang, C. C., Buen, F., Harris, B. T., et al., 2010. ACAT1 gene ablation increases 24(S)-hydroxycholesterol content in the brain and ameliorates amyloid pathology in mice with AD. Proc. Natl. Acad. Sci. U S A 107, 3081-3086.

Burlot, M. A., Braudeau, J., Michaelsen-Preusse, K., Potier, B., Ayciriex, S., et al., 2015. Cholesterol 24-hydroxylase defect is implicated in memory impairments associated with Alzheimer-like Tau pathology. Hum. Mol. Genet. 24, 5965-5976.

Cameron, B., Landreth, G. E., 2010. Inflammation, microglia, and Alzheimer's disease. Neurobiol. Dis. 37, 503-509.

Casali, B. T., Landreth, G. E., 2016. Aβ Extraction from Murine Brain Homogenates. Bio-protocol 6, e1787.

Chali, F., Djelti, F., Eugene, E., Valderrama, M., Marquer, C., et al., 2015. Inhibiting cholesterol degradation induces neuronal sclerosis and epileptic activity in mouse hippocampus. Eur. J. Neurosci. 41, 1345-1355.

Chawla, A., Repa, J. J., Evans, R. M., Mangelsdorf, D. J., 2001. Nuclear receptors and lipid physiology: opening the X-files. Science 294, 1866-1870.

Chen, W., Chen, G., Head, D. L., Mangelsdorf, D. J., Russell, D. W., 2007. Enzymatic reduction of oxysterols impairs LXR signaling in cultured cells and the livers of mice. Cell Metab. 5, 73-79.

Chia, P. Z., Gleeson, P. A., 2011. Intracellular trafficking of the beta-secretase and processing of amyloid precursor protein. IUBMB Life 63, 721-729.

Corona, A. W., Kodoma, N., Casali, B. T., Landreth, G. E., 2016. ABCA1 is Necessary for Bexarotene-Mediated Clearance of Soluble Amyloid Beta from the Hippocampus of APP/PS1 Mice. J. Neuroimmune Pharmacol. 11, 61-72.

Cui, W., Taub, D. D., Gardner, K., 2007. qPrimerDepot: a primer database for quantitative real time PCR. Nucleic Acids Res. 35, D805-809.

Das, S., Potter, H., 1995. Expression of the Alzheimer amyloid-promoting factor antichymotrypsin is induced in human astrocytes by IL-1. Neuron 14, 447-456.
Dickson, D. W., 1997. The pathogenesis of senile plaques. J. Neuropathol. Exp. Neurol. 56, 321-339.
Dietschy, J. M., Turley, S. D., 2004. Thematic review series: brain Lipids. Cholesterol metabolism in the central nervous system during early development and in the mature animal. J. Lipid Res. 45, 1375-1397.
Djelti, F., Braudeau, J., Hudry, E., Dhenain, M., Varin, J., et al., 2015. CYP46A1 inhibition, brain cholesterol accumulation and neurodegeneration pave the way for Alzheimer's disease. Brain 138, 2383-2398.
Eriksson, S., Janciauskiene, S., Lannfelt, L., 1995. Alpha 1-antichymotrypsin regulates Alzheimer beta-amyloid peptide fibril formation. Proc Natl Acad Sci U S A 92, 2313-2317.
Fassbender, K., Simons, M., Bergmann, C., Stroick, M., Lutjohann, D., et al., 2001. Simvastatin strongly reduces levels of Alzheimer's disease beta -amyloid peptides Abeta 42 and Abeta 40 in vitro and in vivo. Proc. Natl. Acad. Sci. U S A 98, 5856-5861.
Ferrera, P., Mercado-Gomez, O., Silva-Aguilar, M., Valverde, M., Arias, C., 2008. Cholesterol potentiates beta-amyloid-induced toxicity in human neuroblastoma cells: involvement of oxidative stress. Neurochem. Res. 33, 1509-1517.
Gamba, P., Leonarduzzi, G., Tamagno, E., Guglielmotto, M., Testa, G., et al., 2011. Interaction between 24-hydroxycholesterol, oxidative stress, and amyloid-beta in amplifying neuronal damage in Alzheimer's disease: three partners in crime. Aging Cell. 10, 403-417.
Ghisletti, S., Huang, W., Ogawa, S., Pascual, G., Lin, M. E., et al., 2007. Parallel SUMOylation-dependent pathways mediate gene- and signal-specific transrepression by LXRs and PPARgamma. Mol. Cell. 25, 57-70.
Gitter, B. D., Boggs, L. N., May, P. C., Czilli, D. L., Carlson, C. D., 2000. Regulation of cytokine secretion and amyloid precursor protein processing by proinflammatory amyloid beta (A beta). Ann. N. Y. Acad. Sci. 917, 154-164.
Grimm, M. O., Grimm, H. S., Patzold, A. J., Zinser, E. G., Halonen, R., et al., 2005. Regulation of cholesterol and sphingomyelin metabolism by amyloid-beta and presenilin. Nat. Cell. Biol. 7, 1118-1123.
Grosgen, S., Grimm, M. O., Friess, P., Hartmann, T., 2010. Role of amyloid beta in lipid homeostasis. Biochim. Biophys. Acta 1801, 966-974.
Guan, F., Gu, J., Hu, F., Zhu, Y., Wang, W., 2012. Association between alpha1-antichymotrypsin signal peptide -15A/T polymorphism and the risk of Alzheimer's disease: a meta-analysis. Mol. Biol. Reports 39, 6661-6669.
Haass, C., Selkoe, D. J., 2007. Soluble protein oligomers in neurodegeneration: lessons from the Alzheimer's amyloid beta-peptide. Nat. Rev. Mol. Cell. Biol. 8, 101-112.
Heit, C., Jackson, B. C., McAndrews, M., Wright, M. W., Thompson, D. C., et al., 2013. Update of the human and mouse SERPIN gene superfamily. Hum. Genomics 7, 22.
Hudry, E., Van Dam, D., Kulik, W., De Deyn, P. P., Stet, F. S., et al., 2010. Adeno-associated virus gene therapy with cholesterol 24-hydroxylase reduces the amyloid pathology before or after the onset of amyloid plaques in mouse models of Alzheimer's disease. Mol. Ther. 18, 44-53.
Janowski, B. A., Willy, P. J., Devi, T. R., Falck, J. R., Mangelsdorf, D. J., 1996. An oxysterol signalling pathway mediated by the nuclear receptor LXR alpha. Nature 383, 728-731.
Joseph, S. B., Castrillo, A., Laffitte, B. A., Mangelsdorf, D. J., Tontonoz, P., 2003. Reciprocal regulation of inflammation and lipid metabolism by liver X receptors. Nat. Med. 9, 213-219.
Kim, O. S., Lee, C. S., Joe, E. H., Jou, I., 2006. Oxidized low density lipoprotein suppresses lipopolysaccharide-induced inflammatory responses in microglia: oxidative stress acts through control of inflammation. Biochem. Biophys. Res. Commun. 342, 9-18.
Kojro, E., Gimpl, G., Lammich, S., Marz, W., Fahrenholz, F., 2001. Low cholesterol stimulates the nonamyloidogenic pathway by its effect on the alpha -secretase ADAM 10. Proc. Natl. Acad. Sci. U S A 98, 5815-5820.
Kolsch, H., Lutjohann, D., Tulke, A., Bjorkhem, I., Rao, M. L., 1999. The neurotoxic effect of 24-hydroxycholesterol on SH-SY5Y human neuroblastoma cells. Brain. Res. 818, 171-175.

Kotti, T., Head, D. D., McKenna, C. E., Russell, D. W., 2008. Biphasic requirement for geranylgeraniol in hippocampal long-term potentiation. Proc. Natl. Acad. Sci. U S A 105, 11394-11399.
Kotti, T. J., Ramirez, D. M., Pfeiffer, B. E., Huber, K. M., Russell, D. W., 2006. Brain cholesterol turnover required for geranylgeraniol production and learning in mice. Proc. Natl. Acad. Sci. U. S. A. 103, 3869-3874.
Langmead, B., Salzberg, S. L., 2012. Fast gapped-read alignment with Bowtie 2. Nat. Methods 9, 357-359.
Lee, J. H., Park, S. M., Kim, O. S., Lee, C. S., Woo, J. H., et al., 2009. Differential SUMOylation of LXRalpha and LXRbeta mediates transrepression of STAT1 inflammatory signaling in IFN-gamma-stimulated brain astrocytes. Mol. Cell 35, 806-817.
Lefterov, I., Bookout, A., Wang, Z., Staufenbiel, M., Mangelsdorf, D., et al., 2007. Expression profiling in APP23 mouse brain: inhibition of Abeta amyloidosis and inflammation in response to LXR agonist treatment. Mol. Neurodegener. 2, 20.
Leone, S., Noera, G., Bertolini, A., 2013. Melanocortins as innovative drugs for ischemic diseases and neurodegenerative disorders: established data and perspectives. Curr. Med. Chem. 20, 735-750.
Lewis, T. L., Cao, D., Lu, H., Mans, R. A., Su, Y. R., et al., 2010. Overexpression of human apolipoprotein A-I preserves cognitive function and attenuates neuroinflammation and cerebral amyloid angiopathy in a mouse model of Alzheimer disease. J. Biol. Chem. 285, 36958-36968.
Licastro, F., Mallory, M., Hansen, L. A., Masliah, E., 1998. Increased levels of alpha-1-antichymotrypsin in brains of patients with Alzheimer's disease correlate with activated astrocytes and are affected by APOE 4 genotype. J. Neuroimmunol. 88, 105-110.
Loffler, T., Flunkert, S., Havas, D., Santha, M., Hutter-Paier, B., et al., 2013. Impact of ApoB-100 expression on cognition and brain pathology in wild-type and hAPPsl mice. Neurobiol. Aging 34, 2379-2388.
Lund, E. G., Guileyardo, J. M., Russell, D. W., 1999. cDNA cloning of cholesterol 24-hydroxylase, a mediator of cholesterol homeostasis in the brain. Proc. Natl. Acad. Sci. U. S. A. 96, 7238-7243.
Lutjohann, D., Breuer, O., Ahlborg, G., Nennesmo, I., Siden, A., et al., 1996. Cholesterol homeostasis in human brain: evidence for an age-dependent flux of 24S-hydroxycholesterol from the brain into the circulation. Proc. Natl. Acad. Sci. U. S. A. 93, 9799-9804.
Lutjohann, D., Papassotiropoulos, A., Bjorkhem, I., Locatelli, S., Bagli, M., et al., 2000. Plasma 24S-hydroxycholesterol (cerebrosterol) is increased in Alzheimer and vascular demented patients. J. Lipid Res. 41, 195-198.
Lutjohann, D., von Bergmann, K., 2003. 24S-hydroxycholesterol: a marker of brain cholesterol metabolism. Pharmacopsychiatry 36 Suppl 2, S102-106.
Ma, J., Brewer, H. B., Jr., Potter, H., 1996. Alzheimer A beta neurotoxicity: promotion by antichymotrypsin, ApoE4; inhibition by A beta-related peptides. Neurobiol. Aging 17, 773-780.
Ma, J., Yee, A., Brewer, H. B., Jr., Das, S., Potter, H., 1994. Amyloid-associated proteins alpha 1-antichymotrypsin and apolipoprotein E promote assembly of Alzheimer beta-protein into filaments. Nature 372, 92-94.
Machein, U., Lieb, K., Hull, M., Fiebich, B. L., 1995. IL-1 beta and TNF alpha, but not IL-6, induce alpha 1-antichymotrypsin expression in the human astrocytoma cell line U373 MG. Neuroreport 6, 2283-2286.
Maes, O. C., Kravitz, S., Mawal, Y., Su, H., Liberman, A., et al., 2006. Characterization of alpha1-antitrypsin as a heme oxygenase-1 suppressor in Alzheimer plasma. Neurobiol. Dis. 24, 89-100.
Maioli, S., Bavner, A., Ali, Z., Heverin, M., Ismail, M. A., et al., 2013. Is it possible to improve memory function by upregulation of the cholesterol 24S-hydroxylase (CYP46A1) in the brain? PLoS One 8, e68534-e68534.
Mast, N., Andersson, U., Nakayama, K., Bjorkhem, I., Pikuleva, I. A., 2004. Expression of human cytochrome P450 46A1 in Escherichia coli: effects of N- and C-terminal modifications. Arch. Biochem. Biophys. 428, 99-108.
Mast, N., Charvet, C., Pikuleva, I. A., Stout, C. D., 2010. Structural basis of drug binding to CYP46A1, an enzyme that controls cholesterol turnover in the brain. J. Biol. Chem. 285, 31783-31795.
Mast, N., Li, Y., Linger, M., Clark, M., Wiseman, J., et al., 2014. Pharmacologic stimulation of cytochrome P450 46A1 and cerebral cholesterol turnover in mice. J. Biol. Chem. 289, 3529-3538.

Mast, N., Liao, W. L., Pikuleva, I. A., Turko, I. V., 2009. Combined use of mass spectrometry and heterologous expression for identification of membrane-interacting peptides in cytochrome P450 46A1 and NADPH-cytochrome P450 oxidoreductase. Arch. Biochem. Biophys. 483, 81-89.
Mast, N., Linger, M., Clark, M., Wiseman, J., Stout, C. D., et al., 2012. In silico and intuitive predictions of CYP46A1 inhibition by marketed drugs with subsequent enzyme crystallization in complex with fluvoxamine. Mol. Pharmacol. 82, 824-834.
Mast, N., Norcross, R., Andersson, U., Shou, M., Nakayama, K., et al., 2003. Broad substrate specificity of human cytochrome P450 46A1 which initiates cholesterol degradation in the brain. Biochemistry 42, 14284-14292.
Mast, N., Reem, R., Bederman, I., Huang, S., DiPatre, P. L., et al., 2011. Cholestenoic acid is an important elimination product of cholesterol in the retina: comparison of retinal cholesterol metabolism with that in the brain. Invest. Ophthalmol. Vis. Sci. 52, 594-603.
Mast, N., Zheng, W., Stout, C. D., Pikuleva, I. A., 2013a. Antifungal azoles: structural insights into undesired tight binding to cholesterol-metabolizing CYP46A1. Mol. Pharmacol. 84, 86-94.
Mast, N., Zheng, W., Stout, C. D., Pikuleva, I. A., 2013b. Binding of a cyano- and fluoro-containing drug bicalutamide to cytochrome P450 46A1: unusual features and spectral response. J. Biol. Chem. 288, 4613-4624.
Mohamed, A., Saavedra, L., Di Pardo, A., Sipione, S., Posse de Chaves, E., 2012. beta-amyloid inhibits protein prenylation and induces cholesterol sequestration by impairing SREBP-2 cleavage. J. Neurosci. 32, 6490-6500.
Moon, M., Song, H., Hong, H. J., Nam, D. W., Cha, M. Y., et al., 2013. Vitamin D-binding protein interacts with Abeta and suppresses Abeta-mediated pathology. Cell Death Differ. 20, 630-638.
Morihara, T., Teter, B., Yang, F., Lim, G. P., Boudinot, S., et al., 2005. Ibuprofen suppresses interleukin-1beta induction of pro-amyloidogenic alpha1-antichymotrypsin to ameliorate beta-amyloid (Abeta) pathology in Alzheimer's models. Neuropsychopharm. 30, 1111-1120.
Namba, Y., Ikeda, K., 1991. [Apolipoprotein B immunoreactivity in cerebral amyloid deposits and neurofibrillary tangles in senile dementia of Alzheimer type]. Rinsho Shinkeigaku 31, 826-830.
Nilsson, L. N., Bales, K. R., DiCarlo, G., Gordon, M. N., Morgan, D., et al., 2001. Alpha-1-antichymotrypsin promotes beta-sheet amyloid plaque deposition in a transgenic mouse model of Alzheimer's disease. J. Neurosci. 21, 1444-1451.
Oakley, H., Cole, S. L., Logan, S., Maus, E., Shao, P., et al., 2006. Intraneuronal beta-amyloid aggregates, neurodegeneration, and neuron loss in transgenic mice with five familial Alzheimer's disease mutations: potential factors in amyloid plaque formation. J. Neurosci. 26, 10129-10140.
Ohno, M., Chang, L., Tseng, W., Oakley, H., Citron, M., et al., 2006. Temporal memory deficits in Alzheimer's mouse models: rescue by genetic deletion of BACE1. Neuropsychopharm. 23, 251-260.
Orsini, C. A., Maren, S., 2012. Neural and cellular mechanisms of fear and extinction memory formation. Neurosci Biobehav Rev 36, 1773-1802.
Paul, S. M., Doherty, J. J., Robichaud, A. J., Belfort, G. M., Chow, B. Y., et al., 2013. The major brain cholesterol metabolite 24(S)-hydroxycholesterol is a potent allosteric modulator of N-methyl-D-aspartate receptors. J. Neurosci. 33, 17290-17300.
Pfrieger, F. W., Ungerer, N., 2011. Cholesterol metabolism in neurons and astrocytes. Prog. Lipid Res. 50, 357-371.
Pierrot, N., Tyteca, D., D'Auria, L., Dewachter, I., Gailly, P., et al., 2013. Amyloid precursor protein controls cholesterol turnover needed for neuronal activity. EMBO Mol. Med. 5, 608-625.
Quan, G., Xie, C., Dietschy, J. M., Turley, S. D., 2003. Ontogenesis and regulation of cholesterol metabolism in the central nervous system of the mouse. Brain Res. Dev. Brain Res. 146, 87-98.
Ramirez, D. M., Andersson, S., Russell, D. W., 2008. Neuronal expression and subcellular localization of cholesterol 24-hydroxylase in the mouse brain. J. Comp. Neurol. 507, 1676-1693.
Rozemuller, J. M., Eikelenboom, P., Stam, F. C., Beyreuther, K., Masters, C. L., 1989. A4 protein in Alzheimer's disease: primary and secondary cellular events in extracellular amyloid deposition. J. Neuropathol. Exp. Neurol. 48, 674-691.

Russell, D. W., Halford, R. W., Ramirez, D. M., Shah, R., Kotti, T., 2009. Cholesterol 24-hydroxylase: an enzyme of cholesterol turnover in the brain. Annu. Rev. Biochem. 78, 1017-1040.
Saijo, K., Crotti, A., Glass, C. K., 2013. Regulation of microglia activation and deactivation by nuclear receptors. Glia 61, 104-111.
Saito, T., Matsuba, Y., Mihira, N., Takano, J., Nilsson, P., et al., 2014. Single App knock-in mouse models of Alzheimer's disease. Nat. Neurosci. 17, 661-663.
Sardi, F., Fassina, L., Venturini, L., Inguscio, M., Guerriero, F., et al., 2011. Alzheimer's disease, autoimmunity and inflammation. The good, the bad and the ugly. Autoimmun. Rev. 11, 149-153.
Schmechel, D. E., Edwards, C. L., 2012. Fibromyalgia, mood disorders, and intense creative energy: A1AT polymorphisms are not always silent. Neurotoxicology 33, 1454-1472.
Schmidt, S. D., Jiang, Y., Nixon, R. A., Mathews, P. M., 2005. Tissue processing prior to protein analysis and amyloid-beta quantitation. Methods Mol. Biol. 299, 267-278.
Schneider, F., Baldauf, K., Wetzel, W., Reymann, K. G., 2014. Behavioral and EEG changes in male 5xFAD mice. Physiol Behav 135, 25-33.
Schwab, C., McGeer, P. L., 2008. Inflammatory aspects of Alzheimer disease and other neurodegenerative disorders. J. Alzheimers Dis. 13, 359-369.
Shafaati, M., Mast, N., Beck, O., Nayef, R., Heo, G. Y., et al., 2010. The antifungal drug voriconazole is an efficient inhibitor of brain cholesterol 24S-hydroxylase (CYP46A1) in vitro and in vivo. J. Lipid Res. 51, 318-323.
Shafaati, M., Olin, M., Bavner, A., Pettersson, H., Rozell, B., et al., 2011. Enhanced production of 24S-hydroxycholesterol is not sufficient to drive liver X receptor target genes in vivo. J. Intern. Med. 270, 377-387.
Simons, M., Keller, P., De Strooper, B., Beyreuther, K., Dotti, C. G., et al., 1998. Cholesterol depletion inhibits the generation of beta-amyloid in hippocampal neurons. Proc. Natl. Acad. Sci. U. S. A. 95, 6460-6464.
Song, F., Poljak, A., Crawford, J., Kochan, N. A., Wen, W., et al., 2012. Plasma apolipoprotein levels are associated with cognitive status and decline in a community cohort of older individuals. PLoS One 7, e34078.
Stanyon, H. F., Viles, J. H., 2012. Human serum albumin can regulate amyloid-beta peptide fiber growth in the brain interstitium: implications for Alzheimer disease. J. Biol. Chem. 287, 28163-28168.
Styren, S. D., Kamboh, M. I., DeKosky, S. T., 1998. Expression of differential immune factors in temporal cortex and cerebellum: the role of alpha-1-antichymotrypsin, apolipoprotein E, and reactive glia in the progression of Alzheimer's disease. J. Comp. Neurol. 396, 511-520.
Sun, M. Y., Izumi, Y., Benz, A., Zorumski, C. F., Mennerick, S., 2016a. Endogenous 24S-hydroxycholesterol modulates NMDAR-mediated function in hippocampal slices. J. Neurophysiol. 115, 1263-1272.
Sun, M. Y., Linsenbardt, A. J., Emnett, C. M., Eisenman, L. N., Izumi, Y., et al., 2016b. 24(S)-Hydroxycholesterol as a Modulator of Neuronal Signaling and Survival. Neuroscientist 22, 132-144.
Trapnell, C., Pachter, L., Salzberg, S. L., 2009. TopHat: discovering splice junctions with RNA-Seq. Bioinformatics 25, 1105-1111.
Trapnell, C., Williams, B. A., Pertea, G., Mortazavi, A., Kwan, G., et al., 2010. Transcript assembly and quantification by RNA-Seq reveals unannotated transcripts and isoform switching during cell differentiation. Nat. Biotechnol. 28, 511-515.
Ulatowski, L., Parker, R., Warrier, G., Sultana, R., Butterfield, D. A., et al., 2014. Vitamin E is essential for Purkinje neuron integrity. Neuroscience 260, 120-129.
Urano, Y., Ochiai, S., Noguchi, N., 2013. Suppression of amyloid-beta production by 24S-hydroxycholesterol via inhibition of intracellular amyloid precursor protein trafficking. Faseb J. 27, 4305-4315.
Van Ess, P. J., Pedersen, W. A., Culmsee, C., Mattson, M. P., Blouin, R. A., 2002. Elevated hepatic and depressed renal cytochrome P450 activity in the Tg2576 transgenic mouse model of Alzheimer's disease. J. Neurochem. 80, 571-578.
Vance, J. E., 2012. Dysregulation of cholesterol balance in the brain: contribution to neurodegenerative diseases. Dis. Model. Mech. 5, 746-755.

Vanmierlo, T., Bloks, V. W., van Vark-van der Zee, L. C., Rutten, K., Kerksiek, A., et al., 2010. Alterations in brain cholesterol metabolism in the APPSLxPS1mut mouse, a model for Alzheimer's disease. J. Alzheimers Dis. 19, 117-127.
Wahrle, S., Das, P., Nyborg, A. C., McLendon, C., Shoji, M., et al., 2002. Cholesterol-dependent gamma-secretase activity in buoyant cholesterol-rich membrane microdomains. Neurobiol. Dis. 9, 11-23.
White, M. A., Mast, N., Bjorkhem, I., Johnson, E. F., Stout, C. D., et al., 2008. Use of complementary cation and anion heavy-atom salt derivatives to solve the structure of cytochrome P450 46A1. Acta Crystallogr. D Biol. Crystallogr. 64, 487-495.
Yu, S., Levi, L., Casadesus, G., Kunos, G., Noy, N., 2014. Fatty acid-binding protein 5 (FABP5) regulates cognitive function both by decreasing anandamide levels and by activating the nuclear receptor peroxisome proliferator-activated receptor beta/delta (PPARbeta/delta) in the brain. J. Biol. Chem. 289, 12748-12758.
Zelcer, N., Khanlou, N., Clare, R., Jiang, Q., Reed-Geaghan, E. G., et al., 2007. Attenuation of neuroinflammation and Alzheimer's disease pathology by liver x receptors. Proc. Natl. Acad. Sci. U S A 104, 10601-10606.
Zhang-Gandhi, C. X., Drew, P. D., 2007. Liver X receptor and retinoid X receptor agonists inhibit inflammatory responses of microglia and astrocytes. J. Neuroimmunol. 183, 50-59.

FIGURE LEGENDS

Fig. 1. Sterol profiles in the brain of B6SJL and 5XFAD mice, EFV untreated (Utx) or treated (Tx). Age-dependent changes were monitored in 1- to 9-month old animals. Gray asterisks are significant changes in Utx 5XFAD mice *vs* the background B6SJL strain; black asterisks are significant changes in Tx 5XFAD mice *vs* Utx 5XFAD mice. The results are mean ± SD of the measurements in individual animals (n=3-7 male mice per group and time point). *, $P \leq 0.05$; **, $P \leq 0.01$; and ***, $P \leq 0.001$ by repeated measures two-way ANOVA followed by a *post hoc* Bonferroni multiple comparison test. *(M-P)* To clearly see the overlaid sterol profiles, the statistical significance data (asterisks) are not indicated in these panels.

Fig. 2. CYP46A1 activation reduces dense-core amyloid plaques in 5-month old EFV-treated mice. A) Representative images of the brain sections (7-10 male mice per group) stained with ThioS (green). Nuclei were detected by propidium iodide and false colored in blue. B6SJL mice served as a negative control. Scale bars are 1 mm. B) Quantification of the Thioflavin S-positive plaques. Error bars indicate SD. *$P \leq 0.05$ by a two-tailed, unpaired Student's t-test.

Fig. 3. CYP46A1 activation reduces diffuse-core amyloid plaques and microglia activation in 5- and 9-month old EFV treated mice. A) Representative images of the brain sections (3-4 male mice per group) showing the anti-6E10 immunoreactivity (red) for diffuse-core amyloid plaques and anti-Iba1 immunoreactivity (green) for activated microglia. Nuclei were stained with DAPI. B6SJL mice served as a negative control. Scale bars are 1 mm. B) Quantification of the 6E10-positive amyloid plaques and Iba1-positive cells. Error bars indicate SD. C and D) Quantification of soluble and insoluble amyloid-β peptides by ELISA. Error bars indicate SD. Only males (n=12-13, colored in blue) were used for the measurements in 5 month-old animals; both males (n=4-5) and females (n=4, colored in pink) were used for the measurements in 9 month-old animals. Rectangles and spheres denote amyloid-$\beta_{1\text{-}42}$ and amyloid-$\beta_{1\text{-}40}$ peptides, respectively. Black asterisks are significant changes between the groups comprised of both males and females; blue asterisks are significant changes between the groups comprised of males only; pink asterisks are significant changes between the groups comprised of females only. *$P \leq 0.05$, **$P \leq 0.01$, ***$P \leq 0.001$, **** $P \leq 0.0001$ by a two-tailed, unpaired Student's t-test.

Fig. 4. EFV effects on behavior in 5- and 9-month old 5XFAD mice. Utx, untreated animals; Tx, treated animals; US, unconditioned stimulus; and CS, conditioned stimulus. Bars represent mean ± SEM. A and D) *, $P \leq 0.05$ by a two-tailed, unpaired Student's t-test. B and C) *, $P \leq 0.05$; and ***, $P \leq 0.001$ by a two-way ANOVA with treatment group and trial factors, followed by a Bonferroni corrections as a *post hoc* comparison if needed.

Fig. 5. Effects of CYP46A1 activation on APP and gene expression. A and D) Representative Western blots (n=6-8 mice per group of 5- and 9-month old males) showing the reduction in the brain levels of APP. The relative APP expression is presented below the Western blot and is normalized per β-actin. At 5 months of age, the APP reduction was statistically significant, $P = 0.03$ by a two-tailed, unpaired Student's t-test. At 9 months of age, the reduction was not significant, $P = 0.15$, and only represents a trend. B) The Volcano plot showing the reductions in the gene expression of EFV-treated *vs* untreated mice as indicated by mRNA sequencing of the whole brain transcriptome. The vertical dashed lines are the boundaries of a 2.5-fold change in gene expression (an arbitrary cut off); the horizontal dashed line is the boundary of the P value of 0.05. Genes with ≥ 2.5-fold change and $q \leq 0.05$ are indicated, and those of pertinence to AD are also colored in orange. Three mice per group were used as biological replicates; all 6 were littermates. C) Quantifications by qPCR confirming a reduction in gene expression in EFV-treated *vs* untreated 5XFAD mice indicated by the transcriptome sequencing. The results are mean ± SD of the measurements in individual mice. E) Representative Western blot (n=7 mice per group) showing the

expression of the APP cleavage fragments C99 and C83. The relative fragment expression is normalized per GAPDH. (F) Quantifications of the C99 and C83 fragments: individual, as a sum (C83 + C99), and as the ratio (C83/C99). Error bars indicate SD. *, $P \leq 0.05$ by a two-tailed, unpaired Student's t-test.

Fig. 6. Proposed model unifying EFV effects. The sequence of events is numbered chronologically with primes (',",''') indicating events that may occur simultaneously. Events in black above black arrows are those supported experimentally by the present work; events in gray above gray arrows are putative and suggested, in most cases, on the basis of literature data. Thin and thick black lines underline events after 4- and 8-months of EFV treatment, respectively. Events 1 and 2: CYP46A1 is the only enzyme in mice that can produce 24HC in the brain (Lund et al., 1999), hence an increase in the brain 24HC levels measured in Fig. 1D-P provides evidence for enzyme activation by EFV. Event 3 is supported by an increase in the brain lathosterol levels triggered by an increase in the 24HC levels (Fig. 1B-N). Events 3' and 4 are supported by a decrease in the APP levels in EFV-treated mice (Fig. 5A,B) as well as the literature data summarized in Discussion ((Brown et al., 2004; Chia and Gleeson, 2011; Simons et al., 1998). Events 3" and 4' are supported by improved performance of EFV-treated mice after 8 months of drug treatment in Morris water maze tasks (Fig. 4B) and also literature data presented in Discussion (Kotti et al., 2008; Kotti et al., 2006; Paul et al., 2013; Sun et al., 2016a). Event 3''' cannot be measured *in vivo* directly, only indirectly by measuring the expression of the target genes in cells of interest. Events 5, 5', and 5": neuroinflammation, a hallmark of Alzheimer's disease brain, is characterized by the presence of activated astrocytes and microglia around amyloid plaques (Akiyama et al., 2000; Cameron and Landreth, 2010; Schwab and McGeer, 2008). LXRs are suggested to exert anti-inflammatory effects in multiple cell type and contexts by inhibiting the transcription of the NF-κB-regulated proinflammatory genes such as *IL-1*β and *TNF*α (Ghisletti et al., 2007). Event 5" is supported by a reduction in brain microglia activation as a result of EFV treatment (Fig. 3A). Event 5 is supported by a lowered *Serpina3k* expression in the whole brain transcriptome of EFV-treated mice (Fig. 5B) and data that in Alzheimer's disease brain and mouse models of this disease, plaque-surrounding activated astrocytes have elevated levels of α-1-antichymotrypsin encoded by *SERPINA3* (Abraham et al., 1988; Licastro et al., 1998; Nilsson et al., 2001), a human ortholog of *Serpina3k*. Events 5' and 6: *Serpina1e and Serpina3k*, the two acute phase genes, are downregulated in EFV-treated mice (Fig. 5B,C) indicating a decrease in inflammatory response in infiltrating brain macrophages and brain astrocytes, respectively (Schmechel and Edwards, 2012; Styren et al., 1998). This downregulation is also consistent with a reduction in brain microglia activation as a result of EFV treatment (Fig. 3A). Furthermore, Events 5' and 6 are supported by a lowered *Serpina3n* expression in APP transgenic mice treated with the synthetic LXR agonist T0901317; these mice have a decrease in insoluble amyloid-β peptide along with a suppression of inflammatory response (Lefterov et al., 2007). The beneficial role of activated LXRs in amyloid pathology is also supported by an increase in amyloid plaque load in APP/presenillin transgenic mice lacking LXRs and showing no inhibition of the inflammatory response of glial cells to amyloid-β fibrils (Zelcer et al., 2007). Finally, Event 7 is supported by the literature data (Abraham and Potter, 1989; Eriksson et al., 1995; Ma et al., 1996; Ma et al., 1994), and Event 8 by amyloid burden reduction in EFV-treated mice (Figs. 3C,D).

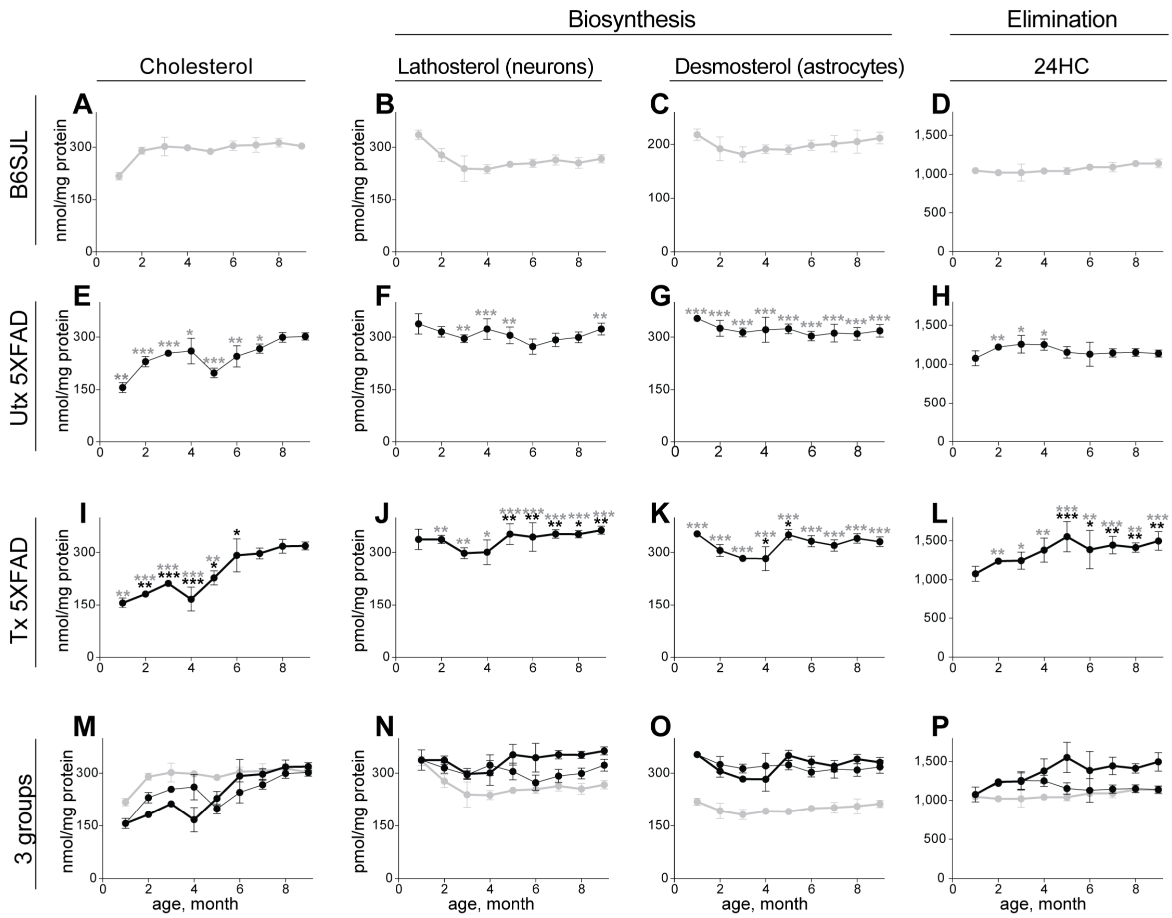

Biosynthesis
Elimination
Cholesterol
Lathosterol (neurons)
Desmosterol (astrocytes)
24HC
B6SJL
Utx 5XFAD
Tx 5XFAD
3 groups
nmol/mg protein
pmol/mg protein
age, month

Fig.1.

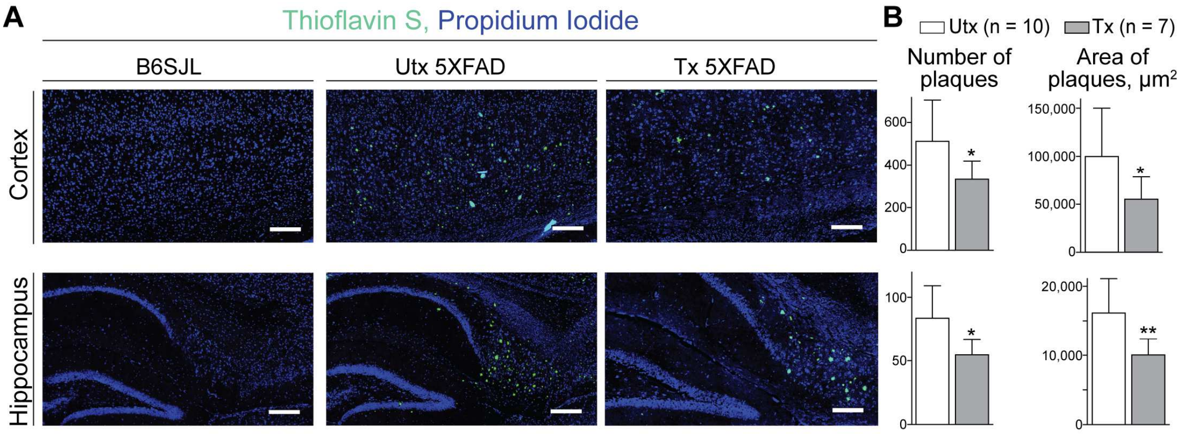
A
Thioflavin S, Propidium Iodide
B6SJL
Utx 5XFAD
Tx 5XFAD
Cortex
Hippocampus
B
Utx (n = 10)
Tx (n = 7)
Number of plaques
Area of plaques, μm2
600
400
200
0
150,000
100,000
50,000
0
100
50
0
20,000
10,000
0
*
**

Fig. 2

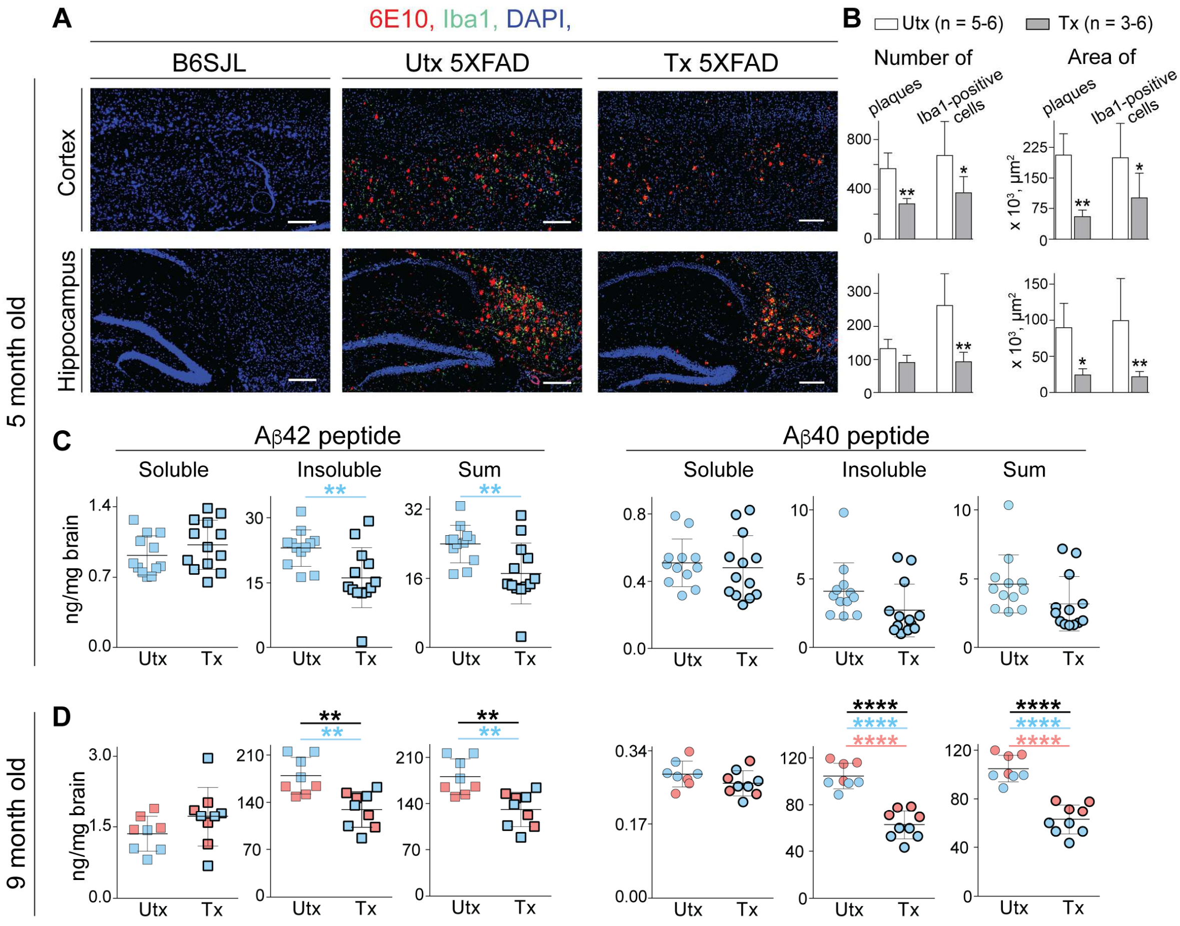
A
6E10, Iba1, DAPI,
B6SJL
Utx 5XFAD
Tx 5XFAD
Cortex
Hippocampus
5 month old
B
Utx (n = 5-6)
Tx (n = 3-6)
Number of
Area of
plaques
Iba1-positive cells
x 10³, µm²
C
Aβ42 peptide
Aβ40 peptide
Soluble
Insoluble
Sum
ng/mg brain
Utx
Tx
D
9 month old

Fig. 3

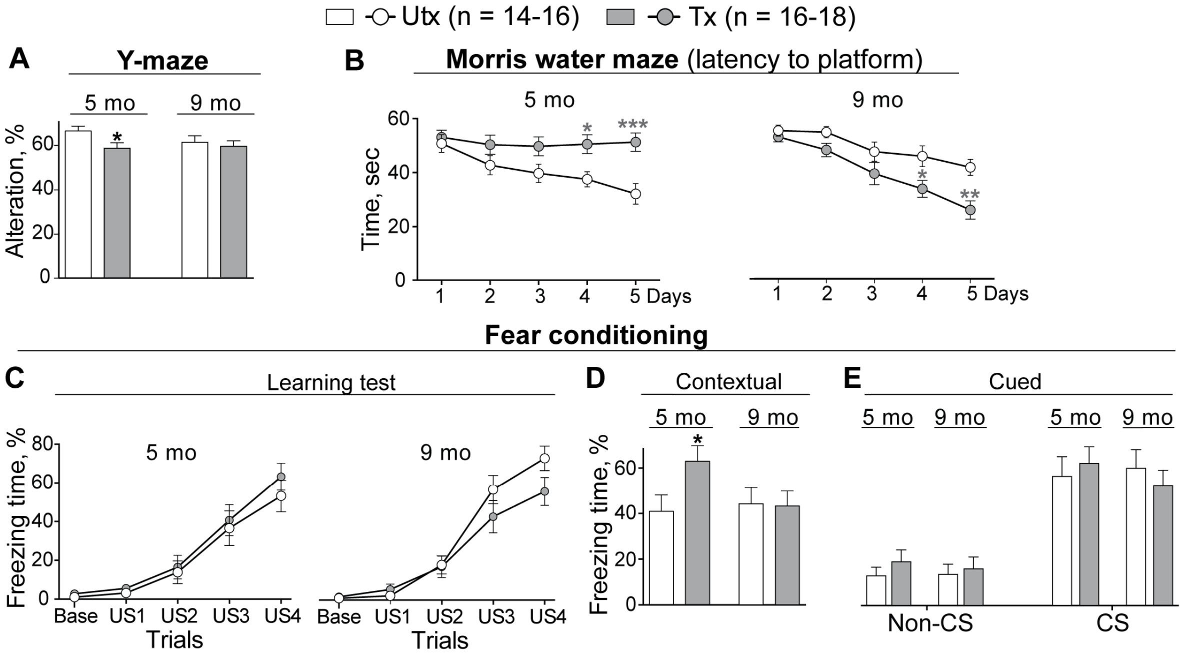

Utx (n = 14-16)
Tx (n = 16-18)
A
Y-maze
5 mo
9 mo
Alteration, %
B
Morris water maze (latency to platform)
5 mo
9 mo
Time, sec
Days
Fear conditioning
C
Learning test
5 mo
9 mo
Freezing time, %
Base
US1
US2
US3
US4
Trials
D
Contextual
5 mo
9 mo
Freezing time, %
E
Cued
5 mo
9 mo
5 mo
9 mo
Non-CS
CS

Fig. 4.

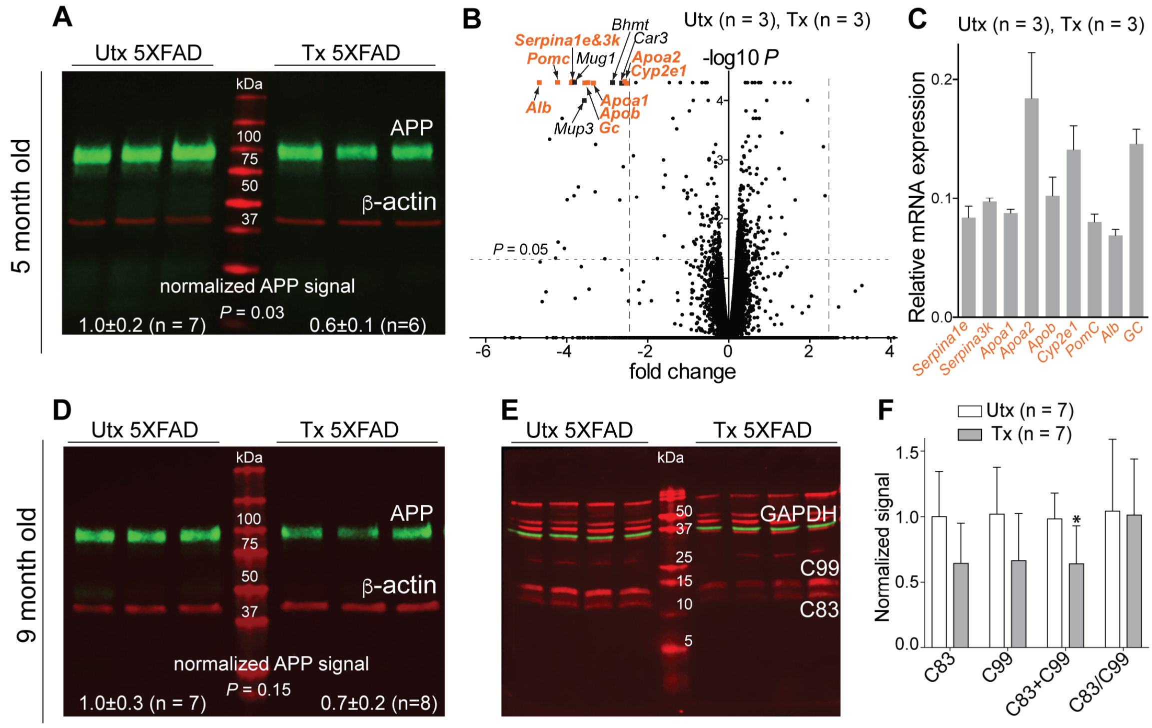
A
Utx 5XFAD
Tx 5XFAD
5 month old
kDa
100
75
50
37
APP
β-actin
normalized APP signal
1.0±0.2 (n = 7)
P = 0.03
0.6±0.1 (n=6)
B
Utx (n = 3), Tx (n = 3)
-log10 P
Serpina1e&3k
Pomc
Mug1
Bhmt
Car3
Apoa2
Cyp2e1
Alb
Apoa1
Apob
Mup3
Gc
P = 0.05
fold change
C
Utx (n = 3), Tx (n = 3)
Relative mRNA expression
Serpina1e
Serpina3k
Apoa1
Apoa2
Apob
Cyp2e1
PomC
Alb
GC
D
Utx 5XFAD
Tx 5XFAD
9 month old
APP
β-actin
normalized APP signal
1.0±0.3 (n = 7)
P = 0.15
0.7±0.2 (n=8)
E
Utx 5XFAD
Tx 5XFAD
GAPDH
C99
C83
F
Utx (n = 7)
Tx (n = 7)
Normalized signal
C83
C99
C83+C99
C83/C99

Fig. 5

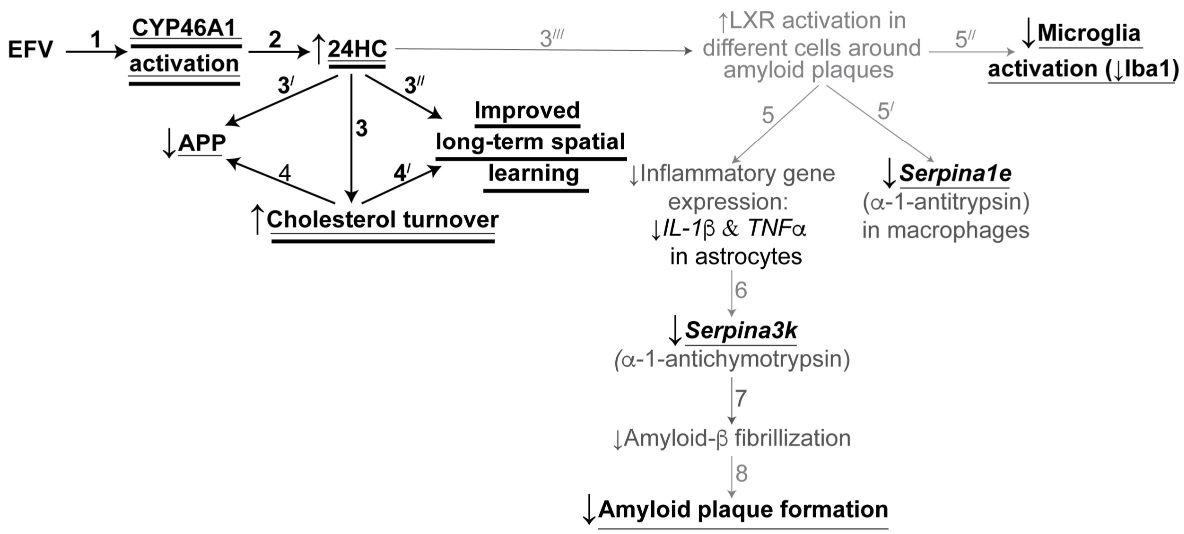

EFV
1
CYP46A1 activation
2
↑24HC
3'
3
3''
3'''
↓APP
Improved long-term spatial learning
4
4'
↑Cholesterol turnover
↑LXR activation in different cells around amyloid plaques
5''
↓Microglia activation (↓Iba1)
5
5'
↓Inflammatory gene expression: ↓IL-1β & TNFα in astrocytes
↓Serpina1e (α-1-antitrypsin) in macrophages
6
↓Serpina3k (α-1-antichymotrypsin)
7
↓Amyloid-β fibrillization
8
↓Amyloid plaque formation

Fig. 6.